Application of near infrared sensors to preconcentration of hydrothermally-formed copper ore

Shekwonyadu Iyakwari[a, *]

si233@exeter.ac.uk

Hylke J. Glass[a]

Gavyn K. Rollinson[a]

Przemyslaw B. Kowalczuk[b]

[a]Camborne School of Mines, University of Exeter, Tremough Campus, Penryn, Cornwall TR10 9FE, UK

[b]Wroclaw University of Technology, Division of Mineral Processing, WybrzezeWyspianskiego 27, 50-370 Wroclaw, Poland

*Corresponding author.

Abstract

Near infrared sensors can be a very useful technique for the qualitative analysis of complex ores, and thus could be useful for the preconcentration of ores. In this paper, individual particles of hydrothermally-formed copper ore sampled from a mine in the Los Pozos mining district, northern Chile, were classified as product, middling and waste based on their near infrared response. The classification of copper bearing minerals (product) from gangue (waste) was considered for vibration combination bands at longer wavelengths from 2000 to 2400 nm. This region exhibits characteristic features for carbonates and hydroxyl gangue bearing minerals. The near infrared features at 1400 and 1900 nm were not considered favourable for classification and subsequent discrimination because they can be influenced by moisture and other environmental factors and are easily suppressed by iron-rich minerals.

Two near infrared preconcentration strategies were applied for particle discrimination. Results indicate that targeting only the calcite (carbonate) dominated particles for discrimination as waste provided the best option for preconcentration. The near infrared discrimination analysis correlates well with mineralogical (QEMSCAN® and XRD) and elemental (XRF) data classification. The results indicate that near infrared spectroscopy is a suitable preconcentration method for supergene copper ore.

Keywords: Preconcentration; Near infrared; QEMSCAN®; XRD; Copper

1 Introduction

Staying ahead of the competition and maintaining profitability is a key challenge in the extractive industry, especially during fluctuating economic conditions. Therefore, it is important to develop novel techniques and strategies for mineral processing which can provide enhanced recovery of the useful components from a low-grade ore, reduce energy consumption and mitigate environmental impacts. A technique which shows promise in such application is Near InfraRed (NIR) spectroscopy (Gaydon et al., 2009; Curtis, 2012; Iyakwari et al., 2013; Dalm et al., 2014; Iyakwari and Glass, 2015).

NIR spectroscopy measures the reflective properties of mineral samples without rigorous sample pre-treatment. It is a fast, non-invasive and non-destructive technique that provides multi-constituent analysis of virtually any matrix (Pasquini, 2003). It covers the wavelength range from the visible range (780 nm) to the mid infrared region (2526 nm) (Clark, 1995; Reich, 2005). The vibrational spectrum of a molecule is a unique physical property (Coates, 2000), thus the NIR could be used as a fingerprint for each pixel of a sample. Furthermore, minerals can be subsequently identified by comparison of the fingerprint spectrum with previously recorded reference spectra of pure minerals. These measurements can hence be used to inform more generic mineral identification and classification methods (Iyakwari et al., 2013).

A major consideration of NIR spectroscopy is the measurement of the reflectance of a pixel which size or position may not correspond to the characteristics of the mineral assembly (Iyakwari and Glass, 2015). In order to obtain a 1:1 correlation between minerals and the NIR spectra, analysis of polished sections of sample particles was carried out using QEMSCAN®. The QEMSCAN® is an automated technique for the rapid characterization of mineral species via combined Scanning Electron Microscopy and Energy Dispersive X-ray Spectrometry (SEM–EDS) (Gottlieb et al., 2000; Pirrie and Rollinson, 2011). The QEMSCAN® allows spatial determination of minerals by the interpretation of chemical spot analyses (Anderson et al., 2014).

The study presented in this paper aims to use NIR sensor-based classification as a tool for the preconcentration of hydrothermally-formed copper samples from associated carbonate and or clay waste. The research was performed with reference to acid leaching as the next and final stage of copper extraction. The preconcentration strategy takes into account the advantage of NIR as a tool for discriminating minerals based on their constituent functional groups (–OH and CO_3^{2-}). Also no two minerals display identical absorption features at the same wavelength positions within the NIR region, even if they contain the same functional groups (Povarennykh, 1978; Iyakwari and Glass, 2014).

Iyakwari and Glass (2015) classified minerals into three major groups, based on their near infrared sensitivity: (a) NIR-active minerals that show absorption features, (b) NIR-active minerals that do not show absorption features, but absorb strongly throughout the longer wavelength region of NIR, and (c) non-active minerals. The non-active minerals do not absorb NIR or display features, even when present in combination with other minerals. Identification of individual minerals in complex particles is influenced by mineral accessibility to radiation, concentration and/or composition (Iyakwari and Glass, 2015). Iyakwari and Glass (2015) showed that the preconcentration of copper-bearing minerals chrysocolla and/or malachite can be achieved by the removal/reduction of calcite and/or muscovite-bearing particles from the feed. The removal of these non-copper bearing NIR-active minerals prior to downstream acid leaching is desirable (Robb, 2005; Iyakwari et al., 2013).

2 Sample characterization and methods

60 particles ranging in size between 5 and 10 cm were selected from a copper ore sampled from a mine in the Los Pozos mining district in the Coastal Range of the Atacama Region, northern Chile. Each of the 60 particles was subjected to the characterization process outlined in Fig. 1.

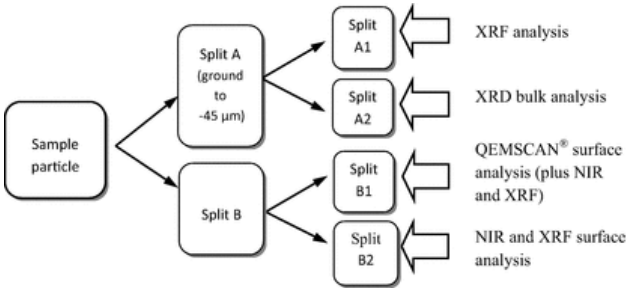

Fig. 1 Subdivision of sample particles for characterization.

Splits A1 and A2 were crushed with a Retsch steel jaw crusher (to –3 mm), then milled to –45 µm using a tungsten-carbide mill prior to X-ray Fluorescence (XRF) and X-ray Diffraction (XRD) analysis respectively. Splits B1 were mounted into ~~Epofix~~ epoxy resin and cut and polished to an even 1 micron finish. The 30 mm diameter polished blocks were marked for orientation and scanned with NIR and Portable X-ray Fluorescence (PXRF). The polished sample blocks were then carbon coated before scanning with the QEMSCAN®. In order to properly map each sample for a 1:1 correlation of NIR and QEMSCAN®, individual mounts were demarcated into three sectors measuring 9 mm each, corresponding to the NIR pixel height with a width of 2.9 mm (Fig. 2). By tracking the position of the individual pixels (spectrum), precise correlation between the NIR spectra and spatial mineralogical data (field scan) from the QEMSCAN® was possible. Splits B2 with sizes ranging from 2 to 10 cm were scanned with the NIR and PXRF without any sample preparation, as the samples were dry and dust free.

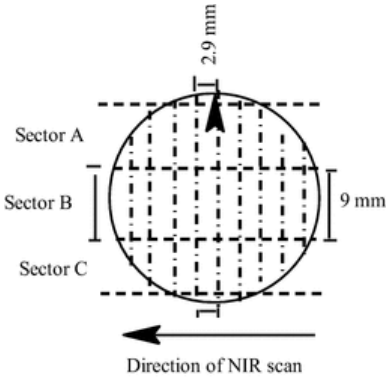

Fig. 2 Split B1 samples (in 30 mm diameter polished blocks) marked for directional scanning and spectral/mineral mapping.

Mineralogical analysis was performed using the QEMSCAN® 4300 system at Camborne School Mines, University of Exeter, UK. Each sample was mapped using the field scan measurement mode, with a beam stepping interval of

10 μm (i.e. an X-ray was acquired every 10 μm across the sample in a grid). This resulted in the acquisition of typically more than 3,500,000 individual X-ray analysis points per sample (i.e. the total number of analysis points, approximately collected per sample, was dependent upon the size/area of the sample as the epoxy resin is ignored). The mineral mass data and an approximate abundance of copper and other elements were based on the assumed average density of each mineral and back-calculated from the QEMSCAN® primary list, where chemical data is supplied manually. Note that the average density and chemistry values were taken from webmineral.com and can only be used as indicative values. A Siemens Bruker D500 XRD analyser (www.bruker.com) was used to semi-qualitatively measure the mineralogical composition of the samples. XRD measurements were matched with known mineral markers using Bruker EVA software. Mineral data obtained from the XRD analysis were compared with the QEMSCAN® data.

The NIR spectra of samples were measured individually with the NIR line scanner, which acquires spectral data on a succession of adjacent area or pixels across the particle surface. Each pixel had dimensions of 2.9 by 9 mm (Fig. 2). Details on NIR background, procedure of NIR data acquisition, instrumentation and data pre-treatment are described in Iyakwari et al. (2013) and Iyakwari and Glass (2015).

Elemental analysis of individual samples were performed using a portable thermos-scientific Niton FXL 950 FM-XRF analyser (PXRF) which was non-destructive requiring little or no sample preparation depending on the material being analysed. The PXRF analyser employs the Energy Dispersive X-ray Spectrometry (EDS) method (www.nitonuk.co.uk).

All analyses (NIR, QEMSCAN®, XRD and PXRF) were performed at the Camborne School of Mines (CSM) laboratory.

3 Results

3.1 Ore mineralogy

There are more than 200 minerals which contain copper in discernible amounts but only a few of them are economically important (Habashi, 1997). The QEMSCAN® mineralogical results presented in Table 1 showed that the main copper bearing mineral in the samples collected from the Los Pozos mining district is chrysocolla ($CuSiO_3 \cdot nH_2O$), which is a silicate mineral of secondary origin. Malachite ($Cu_2(CO_3)(OH)_2$) and cuprite (Cu_2O) occur as traces, with only a few samples containing malachite concentration above 1 wt%.

Table 1 Modal mineralogy of the samples (mass%) measured by QEMSCAN®, <0.01% = below set detection limit.

Sample ID	Silicates										Oxides	Carbonates			Phosphates	Others (trace phases)	Total
	Cu-bearing	Non-Cu-bearing									Cu-bearing	Non-Cu-bearing					
		NIR-active					Non-active			NIR-active	Non-active	NIR-active					
	Chrysocolla	Muscovite	Kaolinite	Biotite	Chlorite	Tourmaline	Quartz	K-feldspar	Plag-feldspar	Hematite	Cuprite	Malachite	Calcite	Ankerite	Apatite		
1	8.33	5.95	0.01	15.54	8.87	0.39	17.69	25.54	0.07	16.63	0.01	<0.01	0.01	0.02	0.18	0.75	100
2	19.05	3.79	0.01	8.32	6.68	0.3	14.96	26.21	0.03	19.9	0.02	<0.01	0.01	0.04	0.27	0.41	100
3	21.11	2.96	0.05	4.53	3.08	0.04	18.16	17.87	0.02	31.77	0.01	0.31	<0.01	<0.01	<0.01	0.10	100
4	5.14	3.28	0.68	7.30	5.13	0.72	6.84	15.50	0.06	55.32	0.01	<0.01	<0.01	<0.01	<0.01	0.02	100
5	3.29	5.34	<0.01	8.38	24.87	0.55	37.88	13.11	0.17	3.72	0.01	1.00	0.02	0.05	0.73	0.90	100
6	1.09	1.00	<0.01	15.32	6.64	0.13	9.86	32.42	1.16	10.37	0.04	0.01	17.17	2.88	0.13	1.78	100
7	0.15	1.55	<0.01	13.01	8.74	0.48	7.46	38.83	0.03	29.03	<0.01	<0.01	0.01	0.06	0.33	0.33	100
8	5.58	0.22	<0.01	5.96	15.76	0.10	4.91	38.01	<0.01	28.47	0.01	<0.01	0.01	0.02	0.16	0.79	100
9	3.98	0.26	<0.01	6.72	14.12	1.49	18.49	4.45	0.41	11.66	0.15	1.38	31.61	4.06	0.31	0.90	100
10	7.78	1.62	<0.01	5.86	4.47	0.13	15.13	1.32	0.01	62.04	0.03	1.55	<0.01	0.01	0.01	0.03	100
11	9.31	2.67	0.33	5.46	4.66	0.18	13.13	20.65	0.08	43.17	<0.01	<0.01	<0.01	<0.01	<0.01	0.36	100
12	6.92	3.55	0.43	4.90	3.47	0.27	11.19	19.44	0.05	49.74	<0.01	<0.01	<0.01	<0.01	<0.01	0.04	100

13	<0.01	2.31	0.02	3.33	2.99	0.06	18.37	11.74	0.30	53.44	<0.01	<0.01	5.08	2.03	<0.01	0.31	100
14	1.19	3.73	1.16	6.71	13.43	2.40	16.14	11.15	0.82	43.06	<0.01	<0.01	0.10	0.05	<0.01	0.07	100
15	<0.01	8.38	0.04	22.89	10.85	0.07	7.69	33.62	0.21	6.98	<0.01	<0.01	3.77	2.64	0.03	2.84	100
16	0.40	0.12	<0.01	9.42	15.16	0.06	38.98	34.25	<0.01	0.63	<0.01	0.01	0.01	<0.01	0.29	0.69	100
17	3.46	0.02	<0.01	0.51	25.61	0.11	64.6	0.76	0.03	3.41	0.02	0.39	0.02	<0.01	0.17	0.90	100
18	0.27	17.73	<0.01	4.59	2.45	0.03	41.9	30.3	0.06	0.22	<0.01	<0.01	1.08	0.64	0.02	0.71	100
19	0.45	9.90	<0.01	17.7	5.37	0.30	20.54	16.95	1.16	7.13	<0.01	<0.01	16.28	2.45	0.25	1.53	100
20	0.81	1.67	<0.01	10.1	36.47	0.36	38.26	10.07	0.05	0.98	0.01	0.14	0.03	<0.01	0.24	0.79	100
21	0.07	18.82	3.11	4.77	4.20	0.25	31.00	16.03	2.26	19.18	<0.01	<0.01	<0.01	<0.01	<0.01	0.31	100
22	0.08	0.25	<0.01	6.99	11.25	0.09	46.08	33.64	0.01	0.12	<0.01	<0.01	0.01	0.01	0.66	0.82	100
23	0.05	0.05	<0.01	1.78	33.81	1.13	57.69	3.13	0.20	0.89	<0.01	<0.01	0.03	0.01	0.21	1.02	100
24	1.23	21.55	<0.01	3.46	1.33	0.05	62.89	5.73	0.03	2.92	0.01	0.66	0.01	0.01	0.07	0.05	100
25	0.36	0.10	<0.01	3.36	17.66	0.47	51.90	4.50	0.30	0.51	<0.01	<0.01	18.81	0.45	0.38	1.21	100
26	3.26	4.14	<0.01	8.47	26.35	0.40	36.34	14.00	0.15	4.13	0.01	1.20	0.02	0.04	0.46	1.04	100
27	<0.01	10.55	0.03	5.08	2.22	0.44	25.81	18.98	3.80	0.18	<0.01	<0.01	28.89	0.27	0.25	3.51	100
28	1.64	<0.01	0.01	0.84	35.08	0.80	57.24	0.10	0.50	1.03	0.01	0.62	0.05	0.01	0.96	1.10	100
29	0.21	14.84	0.02	3.06	1.27	0.51	20.72	11.64	3.51	1.22	<0.01	<0.01	38.82	0.81	0.27	3.10	100
30	0.08	0.14	0.02	3.54	35.29	2.49	50.49	4.38	1.02	1.16	<0.01	<0.01	0.02	0.01	0.39	0.96	100
31	0.27	1.62	<0.01	5.93	45.02	0.36	30.31	10.25	0.12	4.02	<0.01	<0.01	0.05	0.03	0.86	1.16	100
32	2.05	0.22	<0.01	1.16	34.74	0.10	49.57	2.43	0.13	0.74	0.02	0.91	0.35	0.13	4.99	2.47	100
33	<0.01	11.26	0.14	16.28	5.24	0.17	10.64	40.11	0.98	3.05	<0.01	<0.01	8.01	2.13	0.05	1.94	100
34	0.22	0.04	<0.01	1.69	36.54	0.25	56.91	2.32	0.05	0.26	<0.01	<0.01	0.05	0.01	0.35	1.31	100
35	2.98	1.65	<0.01	7.24	19.10	0.06	21.38	10.43	0.26	3.08	0.23	0.85	27.02	4.10	0.53	1.10	100
36	0.02	0.54	<0.01	12.15	16.30	0.06	30.12	34.5	0.07	0.73	<0.01	<0.01	3.78	0.12	0.18	1.43	100
37	0.82	0.08	<0.01	15.69	43.83	0.02	0.40	35.92	<0.01	1.72	<0.01	<0.01	0.01	<0.01	0.21	1.31	100
38	0.18	1.41	<0.01	40.82	7.89	0.17	21.90	22.92	0.05	3.89	<0.01	<0.01	0.03	0.02	0.42	0.31	100
39	0.98	0.11	<0.01	10.24	45.84	0.02	7.89	32.78	0.01	0.27	<0.01	<0.01	0.02	0.01	0.53	1.33	100
40	0.89	0.06	<0.01	1.59	19.61	0.94	72.21	3.8	0.05	0.02	<0.01	<0.01	0.01	<0.01	0.06	0.76	100
41	<0.01	<0.01	0.01	2.95	23.19	9.41	29.54	<0.01	3.99	3.48	<0.01	<0.01	13.1	6.04	0.17	8.12	100
42	0.27	6.12	<0.01	11.81	4.56	0.34	20.31	11.18	1.79	0.43	<0.01	<0.01	40.52	0.56	0.26	1.86	100
43	0.04	4.96	0.10	8.37	6.28	1.58	30.74	10.56	9.08	1.12	<0.01	<0.01	18.45	0.41	0.32	8.00	100
44	0.15	0.21	<0.01	3.14	40.72	0.06	41.10	1.71	0.05	0.35	<0.01	<0.01	10.11	0.25	0.65	1.50	100
45	0.54	0.16	<0.01	7.00	15.58	0.03	3.19	60.96	0.07	2.38	<0.01	<0.01	8.55	0.38	0.22	0.94	100

46	0.13	8.37	0.06	3.91	4.86	1.82	31.37	8.74	7.32	0.95	<0.01	<0.01	25.81	0.51	0.19	5.96	100
47	1.33	0.10	<0.01	2.74	31.10	0.13	30.81	2.59	0.06	4.46	0.03	0.11	22.64	2.42	0.36	1.13	100
48	4.12	1.68	<0.01	8.79	6.65	0.07	10.39	6.53	0.01	59.78	<0.01	<0.01	1.93	0.04	<0.01	0.02	100
49	0.38	12.95	0.03	3.38	1.63	0.88	19.32	10.07	2.84	1.90	0.01	<0.01	42.12	1.29	0.2	2.99	100
50	34.06	0.25	0.01	2.37	16.85	0.05	34.43	10.86	0.01	0.59	0.01	<0.01	0.01	0.24	0.24	0.02	100
51	2.96	2.11	<0.01	14.26	7.08	0.27	14.04	14.81	1.07	9.84	<0.01	<0.01	29.03	0.15	0.15	4.24	100
52	0.04	9.97	<0.01	9.56	4.82	0.19	24.51	7.97	1.44	12.48	<0.01	<0.01	25.01	2.17	0.13	1.69	100
53	0.04	22.16	0.03	2.24	1.04	0.40	24.42	11.96	3.38	0.27	<0.01	<0.01	29.68	0.17	0.24	4–00	100
54	0.19	2.15	0.02	8.37	26.98	1.07	27.35	5.04	3.40	4.32	<0.01	<0.01	16.56	1.77	0.07	2.71	100
55	5.20	18.87	0.05	12.65	5.42	0.62	22.48	4.18	0.89	7.32	0.27	2.21	12.98	5.30	0.54	0.98	100
56	0.13	12.07	<0.01	13.61	12.14	0.53	19.18	9.42	1.14	0.39	<0.01	<0.01	28.53	0.79	0.11	1.95	100
57	6.33	9.90	0.07	9.97	8.39	1.45	23.09	2.49	2.78	8.77	0.25	0.7	17.08	6.46	0.32	1.94	100
58	<0.01	0.87	0.10	6.38	4.68	0.58	4.02	7.88	0.01	75.44	<0.01	<0.01	<0.01	0.01	<0.01	0.04	100
59	0.10	4.58	0.01	18.22	9.95	0.48	11.28	33.24	0.04	21.03	<0.01	<0.01	0.01	0.05	0.31	0.69	100
60	5.84	1.24	0.04	12.89	8.29	0.40	4.13	24.88	0.04	40.00	<0.01	<0.01	1.49	0.53	0.01	0.23	100

The Los Pozos copper ore was rich in silicate minerals, with abundancy ranging from 25% for sample no. 58 to almost 100% for sample no. 40 (Table 1). The most common silicate minerals in the ore in order of abundance were: quartz, feldspar, chlorite, muscovite, biotite, and chrysocolla. Kaolinite and tourmaline were rare, ~~a~~ only sample no. 21 contains high kaolinite (3.11 wt%).

Common carbonate minerals in the investigated ore were calcite and ankerite, with calcite being the most abundant. 21 samples (35% of total) contained calcite above 10 wt% (Table 1). Apatite was the only phosphate mineral in the ore. Only sample no. 32 contained more than 1 wt% apatite. Hematite, ilmenite and cuprite were the only oxide minerals in the ore. While both hematite and ilmenite are iron oxides, cuprite is a copper oxide mineral. Hematite was the dominant oxide mineral in the ore. 13 samples (22% of total) had hematite concentrations above 20 wt% (Table 1).

44 of the 60 samples were analysed by XRD. With the exception of amorphous minerals like chrysocolla and malachite, most of the minerals detected by QEMSCAN® were also identified by the XRD (Table 2) if they occurred in concentrations above the XRD detection limit of approximately 5%. According to Gaydon (2011), a rise in the baseline of XRD pattern with increase in the 2-theta value was indicative of the presence of amorphous or semi-amorphous minerals. Ten samples (no. 1, 2, 3, 6, 8, 9, 10, 11, 24 and 35) showed this rise in the baseline and correlated with their data by QEMSCAN® (Table 1). Hence, the rise in baseline pattern displayed was taken to indicate the presence of chrysocolla.

Table 2 XRD analysis of investigated sub-set of samples. + denotes the presence of mineral in a sample. The amorphous phase is only inferred from XRD patterns with rising baselines.

Sample ID	Quartz	Hematite	Muscovite	Clinochlore (Chlorite)	Calcite	Biotite	K-feldspars		Amorphous Phase
							Microcline	Orthoclase	
1	+	+		+		+		+	+
2	+	+		+				+	+
3	+	+						+	+
4	+	+					+	+	
5	+		+	+			+		
6	+	+		+	+		+		+

7	+	+					+		
8	+	+		+			+		+
9	+			+	+		+		+
10	+	+	+						+
11	+	+					+		+
13	+	+							
14	+	+	+				+		
15	+					+		+	
16	+			+				+	
17	+			+					
18	+		+	+			+		
19	+	+		+	+	+			
20	+		+	+					
21	+	+	+					+	
22	+							+	
24	+	+	+						+
26	+		+	+			+		
27	+		+		+				
28	+			+					
30	+		+	+			+		
31	+		+	+			+		
32	+			+					
34	+			+					
35	+			+	+				+
36	+			+				+	
37	+			+	+			+	
38	+			+		+			
39	+			+			+		
40	+			+			+		
42	+		+	+	+		+		
43	+		+		+				
45	+			+	+			+	
46	+		+		+				

47	+			+	+		+		
56	+			+	+				
57	+		+		+				
58	+	+		+				+	
59	+		+						

Both QEMSCAN® and XRD results showed that in all investigated samples, there were only three major mineral groups: oxides, carbonates and silicates dominated the ore, with phosphate (apatite) occurring as traces.

3.2 Influence of resin used on NIR signal

To check the influence and/or effect of epoxy resin used in the preparation of the samples into mounts for QEMSCAN® mineralogical analysis on the NIR signal, a pure epoxy mount was produced ~~from the Epofix resin~~ and scanned. The NIR signals obtained were treated with the same method as the rock samples and presented in Fig. 3.

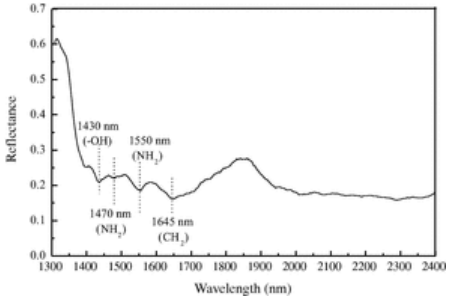

Fig. 3 NIR spectra of Epofix (epoxy resin).

Due to the C–H, O–H and N–H absorption in the NIR region (Bokobza, 1998), the pure ~~Epofix~~ resin block displayed absorption features. The resin exhibits high reflectance at shorter wavelengths between 1308 and 1394 nm and also displays an –OH absorption feature near 1430 nm, NH_2 features near 1470 and 1550 nm and epoxy terminal CH_2 features near 1645 nm. All absorption features correspond to the findings reported by Li et al. (2008). On comparison with the minerals spectra, it was observed that there is a strong contrast between the NIR signals of pure resin and ore particles. Therefore, identification and discrimination of mineral signals from resin signals was possible. None of the wavelength bands associated with absorption features of the resin were selected for preconcentration of the investigated ore.

The average particle size for all investigated samples (split B1, Fig. 1) was ~~from~~ 2.0 to 2.7 cm in width. Therefore, given the pixel size of 2.9 by 9 mm for the NIR, each sample generated between 6 and 9 pixels per sector (Fig. 2). Due to the uneven nature of some particles edges, the resin contributed to a sample edge effect. Hence, such edge pixels were removed from the particles spectra during spectral pre-treatment. Their removal did not affect spectral data interpretations as they were edge pixels and thus not optimal for analysis.

3.3 NIR-active functional groups

The NIR examines minerals based on their functional group(s) (Clark, 1995; Hunt, 1977; Iyakwari and Glass, 2015). The functional groups of interest for the present study were –OH and CO_3^{2-}. The minerals containing these group(s) in the ore include calcite, ankerite and malachite for CO_3^{2-}, and muscovite, kaolinite, biotite, chrysocolla, malachite, chlorite, tourmaline and apatite for OH, (Table 1). Though NIR absorption features produced by malachite are largely due to their CO_3^{2-} functional group (Clark et al., 2007; Iyakwari and Glass, 2015), the –OH group of malachite was also considered. And while hematite does not contain either group, it is considered because of its known high NIR spectral absorption across the wavelength range (Van Der Meer, 1995; Bishop and Dummel, 1996; Iyakwari and Glass, 2015). It is important to note that functional groups like CO_3^{2-} tend to consume acid while groups like –OH, especially the clays, adsorb acid (Gupta, 2003; Curtis, 2012).

All calculations for bulk functional groups are done with reference to values from webmineral.com (Table 3). Analysis of the 60 samples, reveal that only 29 samples contain the CO_3^{2-} functional group, and that CO_3^{2-} is dominantly present in the form of calcite (Tables 1 and 3). All 60 samples contain the –OH functional group (Table 3). With the exception of sample no. 50 which owes its high –OH concentration to chrysocolla (34%), contributing about 7% of its 11% cumulative –OH, all the other high –OH containing samples are dominantly as a result of their chlorite concentration (Table 3). Hematite was detected in all samples, with only 16 samples showing hematite below 1 wt% (Table 1).

Table 3 Calculated modal composition (wt%) of NIR-active functional groups and copper, with reference to webmineral.com (2015). Where HCu = High copper (⩾0.5%), LCu = Low copper (<0.5%), HC = High carbonate (⩾2%), LC = Low carbonate (<2%), HOH = High Hydroxyl (⩾5%), LOH = Low Hydroxyl (<5%), HH = High Hematite (⩾10%), and LH = Low Hematite (<10%).

Sample ID	Hydroxyls									Carbonates		Cumulative -OH	Cumulative CO_3^{2-}	Copper	Classification		
	Muscovite 8.53% (–OH)	Biotite 7.84% (–OH)	Kaolinite 26.34% (–OH)	Chlorite 22.85% (–OH)	Tourmaline 6.61% (–OH)	Chrysocolla 20.71% (–OH)	Apatite 3.34% (–OH)	Malachite 15.38% (–OH) and 27.13% (CO_3^{2-})		Calcite 59.95% (CO_3^{2-})	Ankerite 58.14% (CO_3^{2-})				Copper – CO_3^{2-}	Copper – –OH	Copper – Hematite
								–OH	CO_3^{2-}								
1	0.51	1.22	0.00	2.03	0.03	1.73	0.01	0.00	0.00	0.01	0.01	5.53	0.02	2.83	HCu-LC	HCu-HOH	HCu-HH
2	0.32	0.65	0.00	1.53	0.02	3.95	0.01	0.00	0.00	0.00	0.03	6.48	0.03	6.46	HCu-LC	HCu-HOH	HCu-HH
3	0.25	0.35	0.01	0.70	0.00	4.37	0.00	0.05	0.08	0.00	0.00	5.73	0.08	7.33	HCu-LC	HCu-HOH	HCu-HH
4	0.28	0.57	0.18	1.17	0.05	1.06	0.00	0.00	0.00	0.00	0.00	3.31	0.00	1.75	HCu-LC	HCu-LOH	HCu-HH
5	0.46	0.66	0.00	5.68	0.04	0.68	0.02	0.15	0.27	0.01	0.03	7.69	0.31	1.70	HCu-LC	HCu-HOH	HCu-LH
6	0.09	1.20	0.00	1.52	0.01	0.23	0.00	0.00	0.00	10.29	1.67	3.05	11.96	0.41	LCu-HC	LCu-LOH	LCu-HH
7	0.13	1.02	0.00	2.00	0.03	0.03	0.01	0.00	0.00	0.01	0.03	3.22	0.04	0.05	LCu-LC	LCu-LOH	LCu-HH
8	0.02	0.47	0.00	3.6	0.01	1.16	0.01	0.00	0.00	0.00	0.01	5.27	0.01	1.90	HCu-LC	HCu-HOH	HCu-HH
9	0.02	0.53	0.00	3.23	0.10	0.82	0.01	0.21	0.37	18.95	2.36	4.92	21.68	2.28	HCu-HC	HCu-LOH	HCu-HH
10	0.14	0.46	0.00	1.02	0.01	1.61	0.00	0.24	0.42	0.00	0.01	3.48	0.43	3.55	HCu-LC	HCu-LOH	HCu-HH
11	0.23	0.43	0.09	1.06	0.01	1.93	0.00	0.00	0.00	0.00	0.00	3.75	0.00	3.15	HCu-LC	HCu-LOH	HCu-HH
12	0.30	0.38	0.11	0.79	0.02	1.43	0.00	0.00	0.00	0.00	0.00	3.03	0.00	2.34	HCu-LC	HCu-LOH	HCu-HH
13	0.20	0.26	0.01	0.68	0.00	0.00	0.00	0.00	0.00	3.04	1.18	1.15	4.22	0.00	LCu-HC	LCu-LOH	LCu-HH
14	0.32	0.53	0.31	3.07	0.16	0.25	0.00	0.00	0.00	0.06	0.03	4.64	0.09	0.40	LCu-LC	LCu-LOH	LCu-HH
15	0.72	1.79	0.01	2.48	0.00	0.00	0.00	0.00	0.00	2.26	1.53	5.00	3.79	0.00	LCu-HC	LCu-HOH	LCu-LH
16	0.01	0.74	0.00	3.46	0.00	0.08	0.01	0.00	0.00	0.00	0.00	4.30	0.00	0.14	LCu-LC	LCu-LOH	LCu-LH
17	0.00	0.04	0.00	5.85	0.01	0.72	0.01	0.06	0.10	0.01	0.00	6.69	0.11	1.41	HCu-LC	HCu-HOH	HCu-LH

18	1.51	0.36	0.00	0.56	0.00	0.06	0.00	0.00	0.00	0.65	0.37	2.49	1.02	0.09	LCU-LC	LCu-LOH	LCu-LH
19	0.84	1.39	0.00	1.23	0.02	0.09	0.01	0.00	0.00	9.76	1.42	3.58	11.18	0.15	LCu-HC	LCu-LOH	LCu-LH
20	0.14	0.79	0.00	8.33	0.02	0.17	0.01	0.02	0.04	0.02	0.00	9.48	0.06	0.36	LCu-LC	LCu-HOH	LCu-LH
21	1.61	0.37	0.82	0.96	0.02	0.01	0.00	0.00	0.00	0.00	0.00	3.79	0.00	0.02	LCu-LC	LCu-LOH	LCu-HH
22	0.02	0.55	0.00	2.57	0.01	0.02	0.02	0.00	0.00	0.01	0.01	3.19	0.02	0.03	LCu-LC	LCu-LOH	LCu-LH
23	0.00	0.14	0.00	7.72	0.07	0.01	0.01	0.00	0.00	0.02	0.01	7.95	0.03	0.02	LCu-LC	LCu-HOH	LCu-LH
24	1.84	0.27	0.00	0.30	0.00	0.25	0.00	0.10	0.18	0.00	0.01	2.76	0.19	0.80	HCu-LC	HCu-LOH	HCu-LH
25	0.01	0.26	0.00	4.04	0.03	0.07	0.01	0.00	0.00	11.28	0.26	4.42	11.54	0.12	LCu-HC	LCu-LOH	LCu-LH
26	0.35	0.66	0.00	6.02	0.03	0.68	0.02	0.19	0.33	0.01	0.02	7.95	0.36	1.81	HCu-LC	HCu-HOH	HCu-LH
27	0.90	0.40	0.01	0.51	0.03	0.00	0.01	0.00	0.00	17.32	0.16	1.86	17.48	0.00	LCu-HC	LCu-LOH	LCu-LH
28	0.00	0.07	0.00	8.02	0.05	0.34	0.03	0.10	0.17	0.03	0.01	8.61	0.21	0.92	HCu-LC	HCu-HOH	HCu-LH
29	1.27	0.24	0.01	0.29	0.03	0.04	0.01	0.00	0.00	23.27	0.47	1.89	23.74	0.07	LCu-HC	LCu-LOH	LCu-LH
30	0.01	0.28	0.00	8.06	0.16	0.02	0.01	0.00	0.00	0.01	0.01	8.54	0.02	0.03	LCu-LC	LCu-HOH	LCu-LH
31	0.14	0.46	0.00	10.29	0.02	0.06	0.03	0.00	0.00	0.03	0.02	11.00	0.05	0.09	LCu-LC	LCu-HOH	LCu-LH
32	0.02	0.09	0.00	7.94	0.01	0.42	0.17	0.14	0.25	0.21	0.07	8.79	0.53	1.23	HCu-LC	HCu-HOH	HCu-LH
33	0.96	1.28	0.04	1.20	0.01	0.00	0.00	0.00	0.00	4.80	1.24	3.49	6.04	0.00	LCu-HC	LCu-LOH	LCu-LH
34	0.00	0.13	0.00	8.35	0.02	0.05	0.01	0.00	0.00	0.03	0.01	8.56	0.04	0.07	LCu-LC	LCu-HOH	LCu-LH
35	0.14	0.57	0.00	4.36	0.00	0.62	0.02	0.13	0.23	16.2	2.38	5.84	18.81	1.71	HCu-HC	HCu-HOH	HCu-LH
36	0.05	0.95	0.00	3.73	0.00	0.00	0.01	0.00	0.00	2.26	0.07	4.74	2.33	0.01	LCu-HC	LCu-LOH	LCu-LH
37	0.01	1.23	0.00	10.02	0.00	0.17	0.01	0.00	0.00	0.00	0.00	11.44	0.00	0.28	LCu-LC	LCu-HOH	LCu-LH
38	0.12	3.20	0.00	1.80	0.01	0.04	0.01	0.00	0.00	0.02	0.01	5.18	0.03	0.06	LCu-LC	LCu-HOH	LCu-LH

39	0.01	0.80	0.00	10.47	0.00	0.20	0.02	0.00	0.00	0.01	0.00	11.5	0.01	0.33	LCu-LC	LCu-HOH	LCu-LH
40	0.01	0.12	0.00	4.48	0.06	0.18	0.00	0.00	0.00	0.01	0.00	4.85	0.01	0.3	LCu-LC	LCu-LOH	LCu-LH
41	0.00	0.23	0.00	5.30	0.62	0.00	0.01	0.00	0.00	7.85	3.51	6.16	11.36	0.00	LCu-HC	LCu-HOH	LCu-LH
42	0.52	0.93	0.00	1.04	0.02	0.06	0.01	0.00	0.00	24.29	0.33	2.58	24.62	0.09	LCu-HC	LCu-LOH	LCu-LH
43	0.42	0.66	0.03	1.43	0.10	0.01	0.01	0.00	0.00	11.06	0.24	2.66	11.30	0.01	LCu-HC	LCu-LOH	LCu-LH
44	0.02	0.25	0.00	9.30	0.00	0.03	0.02	0.00	0.00	6.06	0.15	9.62	6.21	0.05	LCu-HC	LCu-HOH	LCu-LH
45	0.01	0.55	0.00	3.56	0.00	0.11	0.01	0.00	0.00	5.13	0.22	4.24	5.35	0.18	LCu-HC	LCu-LOH	LCu-LH
46	0.71	0.31	0.02	1.11	0.12	0.03	0.01	0.00	0.00	15.47	0.30	2.31	15.77	0.04	LCu-HC	LCu-LOH	LCu-LH
47	0.01	0.21	0.00	7.11	0.01	0.28	0.01	0.02	0.03	13.57	1.41	7.65	15.01	0.54	HCu-HC	HCu-HOH	HCu-LH
48	0.14	0.69	0.00	1.52	0.00	0.85	0.00	0.00	0.00	1.16	0.02	3.20	1.18	1.40	HCu-LC	HCu-LOH	HCu-HH
49	1.10	0.26	0.01	0.37	0.06	0.08	0.01	0.00	0.00	25.25	0.75	1.89	26.00	0.14	LCu-HC	LCu-LOH	LCu-LH
50	0.02	0.19	0.00	3.85	0.00	7.05	0.01	0.00	0.00	0.00	0.14	11.12	0.14	11.54	HCu-LC	HCu-HOH	HCu-LH
51	0.18	1.12	0.00	1.62	0.02	0.61	0.00	0.00	0.00	17.41	0.08	3.55	17.49	1.00	HCu-HC	HCu-LOH	HCu-LH
52	0.85	0.75	0.00	1.10	0.01	0.01	0.00	0.00	0.00	15.00	1.26	2.72	16.26	0.01	LCu-HC	LCu-LOH	LCu-HH
53	1.89	0.18	0.01	0.24	0.03	0.01	0.01	0.00	0.00	17.79	0.10	2.37	17.89	0.01	LCu-HC	LCu-LOH	LCu-LH
54	0.18	0.66	0.01	6.17	0.07	0.04	0.00	0.00	0.00	9.93	1.03	7.13	10.96	0.06	LCu-HC	LCu-HOH	LCu-LH
55	1.61	0.99	0.01	1.24	0.04	1.08	0.02	0.34	0.60	7.78	3.08	5.33	11.46	3.28	HCu-HC	HCu-HOH	HCu-LH
56	1.03	1.07	0.00	2.77	0.04	0.03	0.00	0.00	0.00	17.1	0.46	4.94	17.56	0.05	LCu-HC	LCu-LOH	LCu-LH
57	0.84	0.78	0.02	1.92	0.1	1.31	0.01	0.11	0.19	10.24	3.75	5.09	14.18	2.77	HCu-HC	HCu-HOH	HCu-LH
58	0.07	0.50	0.03	1.07	0.04	0.00	0.00	0.00	0.00	0.00	0.01	1.71	0.01	0.00	LCu-LC	LCu-LOH	LCu-HH
59	0.39	1.43	0.00	2.27	0.03	0.02	0.01	0.00	0.00	0.01	0.03	4.15	0.04	0.03	LCu-LC	LCu-LOH	LCu-HH

60	0.11	1.01	0.01	1.89	0.03	1.21	0.00	0.00	0.00	0.89	0.31	4.26	1.20	1.98	HCu-LC	HCu-LOH	HCu-HH

A copper cut-off grade of 0.5% and carbonate cut-off of 2% are assumed. Given its relative abundance, calcite was selected as the main carbonate mineral in the ore. From Table 3, based on copper-carbonate concentration, samples can be classified into 4 groups. 6 samples were classified as high copper-high carbonate samples, 17 samples and were classified as high copper-low carbonate. 20 samples were classified as high carbonate-low copper samples, while 17 samples were classified as low copper-low carbonate samples.

On the basis of copper-hydroxyl ratios, assuming a copper cut-off grade of 0.5% and 5% for –OH (note that the high –OH percentage of 5% taken is to make allowance for the –OH contributed by both chrysocolla and malachite), 9 samples, were classified as high copper-low –OH. 14 samples as high copper-high –OH, while 12 samples were classified as low copper-high –OH. 25 samples were classified as low copper-low-OH samples (Table 3).

Given that chrysocolla was the main copper bearing mineral in the ore and chrysocolla NIR features are only visible in mixtures with a chrysocolla:hematite ratio of 9:1 (Iyakwari and Glass, 2015) and assuming a cut-off grade of 10 wt% for hematite, 11 samples were classified as high copper-high hematite, 12 samples as high copper-low hematite, 8 samples as high hematite-low copper and 29 samples as low copper-low hematite samples (Table 3).

Comparing the various classifications above, the following groups and samples could be considered for economic preconcentration:

i. High copper–low carbonate (sample no. 1, 2, 3, 4, 5, 8, 10, 11, 12, 17, 24, 26, 28 32, 48, 50 and 60).

ii. High copper–low –OH (sample no. 4, 9, 10, 11, 12, 24, 48, 51 and 60).

iii. High copper–high hematite (sample no. 1, 2, 3, 4, 8, 9, 10, 11, 12, 48 and 60) and

iv. High copper–low hematite (sample no. 5, 17, 24, 26, 28, 32, 35, 47, 50, 51, 55 and 57).

Combining all the above groups, ideally on the basis of copper concentration, 23 samples (no. 1, 2, 3, 4, 5, 8, 9, 10, 11, 12, 17, 24, 26, 28, 32, 35, 47, 48, 50, 51, 55, 57 and 60) should be targeted for preconcentration as they contain at least 0.5% Cu. However, some of these samples contain either high CO_3^{2-} and/or high –OH, which is undesirable in downstream leaching.

Since sample no. 1, 2, 3, 5, 9, 17, 26, 28, 32, 35, 47, 50, 51, 55 and 57 have either or both high CO_3^{2-} or high –OH concentration, only sample no. 4, 8, 10, 11, 12, 24, 48 and 60 (13% of total) were considered suitable for preconcentration. This strategy shall be referred to as Func. (1).

It should be noted that chrysocolla contributes 63.4% of the total –OH in sample no. 50. Assuming that chrysocolla always contributes significantly to the –OH content, increasing the allowable –OH content can lead to a higher recovery of copper.

On that basis, the low carbonate-high –OH samples (no. 1, 2, 3, 5, 17, 26, 28, 32, and 50) were added to the target batch. This second strategy, Func. (2),only targets high CO_3^{2-} bearing particles for removal. On this basis, the following samples can now be targeted: no. 1, 2, 3, 4, 5, 8, 10, 11, 12, 17, 24, 26, 28, 32, 48, 50 and 60. This increases the yield to 28% of the particles at the cost of increasing dilution.

3.4 Samples NIR spectral correlation and interpretation

The objective of most mineral processing operations is to separate minerals into two or more fractions based on their economic value (Wills and Napier Munn, 2006; Iyakwari and Glass, 2015). Therefore, given that the dominant copper bearing mineral is chrysocolla with minor malachite, samples are classified based on their NIR spectra signature with reference to strategies by Iyakwari and Glass (2015). Two strategies were developed.

The first strategy, NIR (1), presented in Fig. 4 refers to copper-bearing minerals which contains a hydroxyl (Chrysocolla) or carbonate (Malachite) group associated with high iron bearing minerals (hematite). This strategy targeted the identification of both calcite and clay (muscovite/kaolinite) particles for later removal by assuming that hematite completely masks chrysocolla features. On this basis samples are classified into three groups as:

i. Products – the samples with all NIR spectra showing chrysocolla and/or hematite, chlorite, biotite pattern. This group includes featureless NIR spectra.

ii. Waste – the samples with all NIR spectra showing calcite and or muscovite characteristic spectra.

iii. Middlings – the samples with NIR spectra containing individual spectra of both waste and product groups. This is likely since individual mineral grains are smaller than the pixel size of 2.9 by 9 mm, and particles scanned consisted of at least two pixels (which may be distinct). This group may require further liberation to a size not less than the pixel size and rescanned.

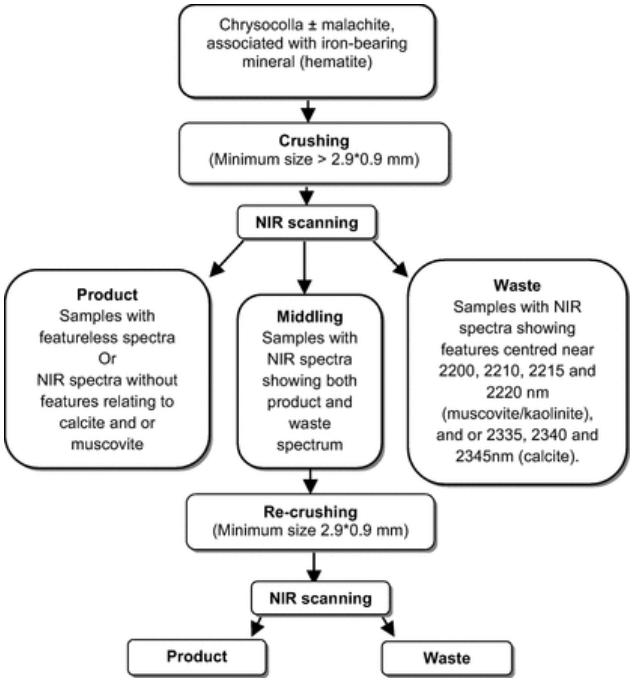

Fig. 4 Copper samples preconcentration strategy NIR (1), targeted at discriminating both calcite and muscovite (clay) bearing particles as waste (modified from Iyakwari and Glass, 2015).

The second strategy, NIR(2), presented in Fig. 5 refers to copper-bearing minerals that contain a hydroxyl group (chrysocolla) not associated with high iron bearing minerals. Hence, the strategy targets only calcite for discrimination. Therefore, individual ore particles shall be classified into three groups as:

i. Waste – the samples with all NIR spectra showing calcite characteristics absorption features.

ii. Products – the samples with all NIR spectra not displaying calcite absorption features.

iii. Middlings – the samples with NIR spectra containing individual spectra of both waste and product groups.

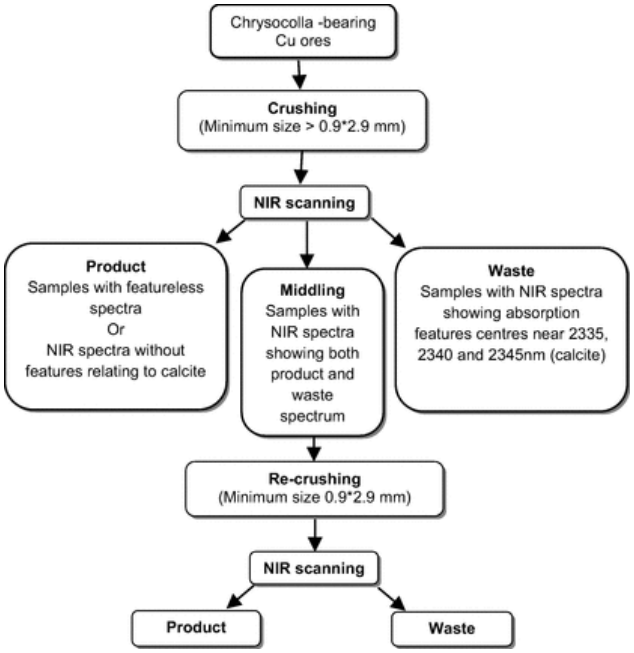

Fig. 5 Copper samples preconcentration strategy NIR (2) targeted at eliminating only calcite-bearing samples as waste (modified from Iyakwari and Glass, 2015).

3.4.1 Individual sample description

Five representative samples (no. 6 (Fig. 6), no. 7 (Fig. 7), no. 9 (Fig. 8), no. 21 (Fig. 9) and no. 49 (Fig. 10) of the 60 split B1 samples are described here in detail. Major absorption features, absorption wavelength position, correlation with reference spectra, and the possible mineral(s) responsible for the absorption features are correlated with mineral data and field scan images. Comparison of classification with PXRF data is presented in Table 4.

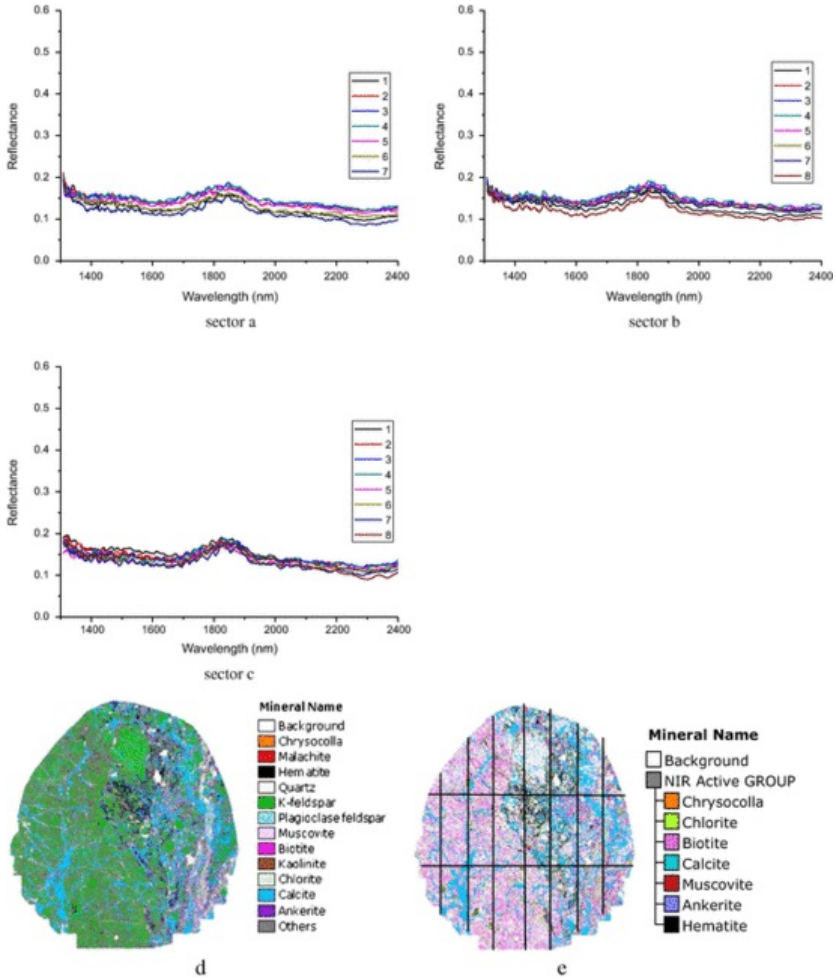

Fig. 6 (Sectors a–c) NIR spectra of sample no. 6. (d and e) The QEMSCAN® field scan image of sample no. 6 at 10 μm X-ray resolution, (d) all minerals present in the sample, (e) NIR-active minerals shown only. Vertical lines indicate pixel position while horizontal lines indicate spectral sectors on particles as scanned.

ELSEVIER_MINE_4780

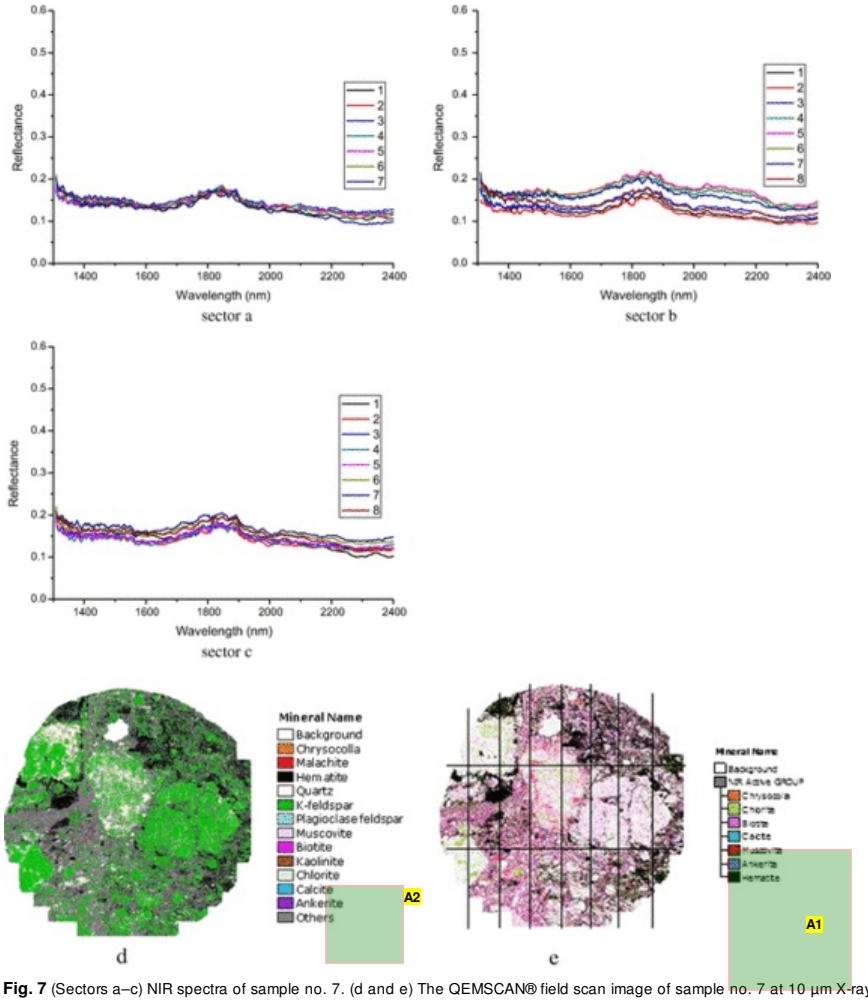

Fig. 7 (Sectors a–c) NIR spectra of sample no. 7. (d and e) The QEMSCAN® field scan image of sample no. 7 at 10 μm X-ray resolution, (b) all minerals present in the sample, (c) NIR active minerals shown only. Vertical lines indicate pixel position while horizontal lines indicate spectral sectors on particles as scanned.

Annotations:

A1. enlarge

A2. MC: Fig correction

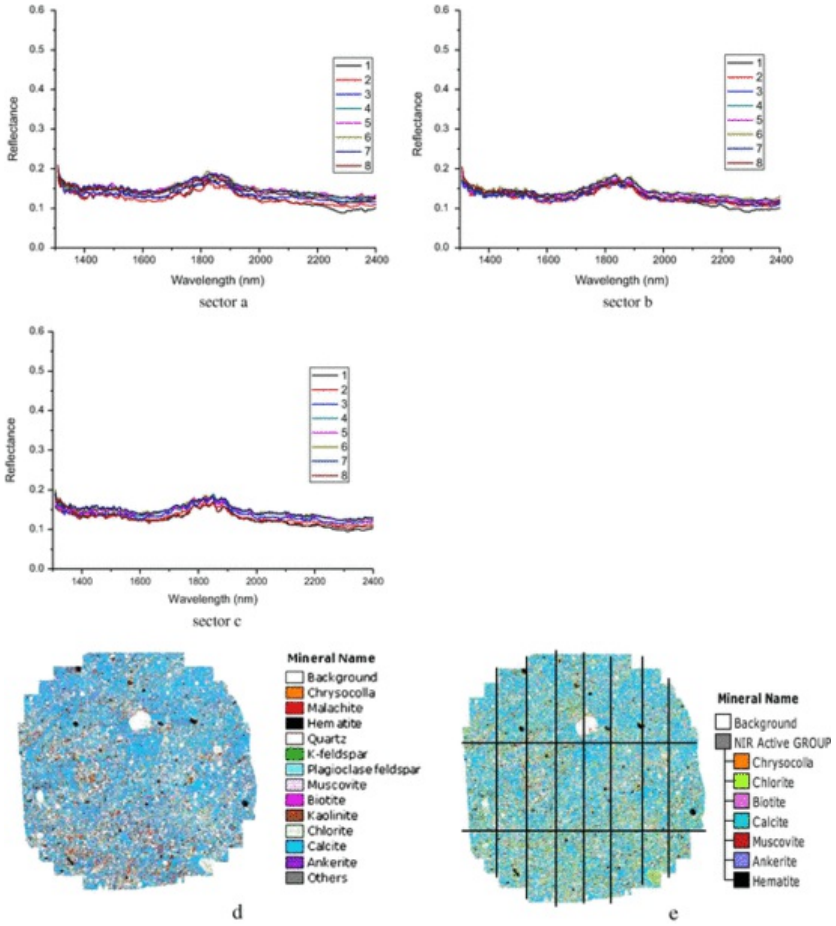

Fig. 8 (a–c) NIR spectra of sample no. 9. (d and e) The QEMSCAN® field scan image of sample no. 9 at 10 μm X-ray resolution, (d) all minerals present in the sample, (e) NIR-active minerals shown only. Vertical lines indicate pixel position while horizontal lines indicate spectral sectors on particles as scanned.

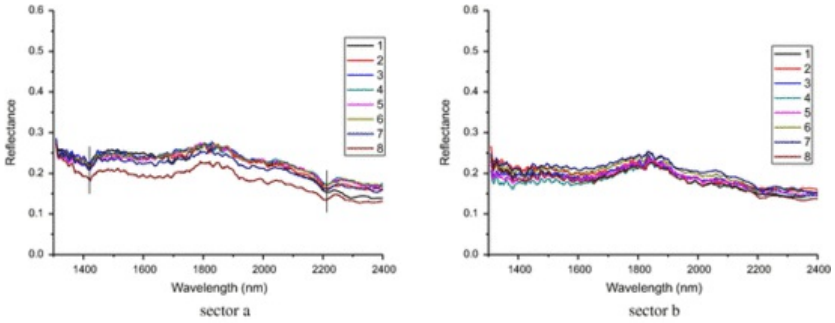

sector a

sector b

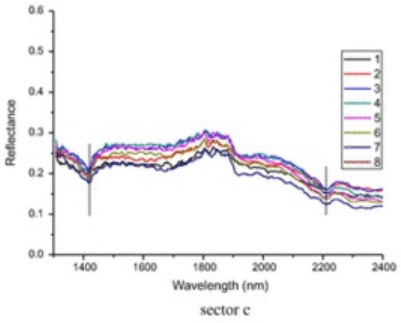

sector c

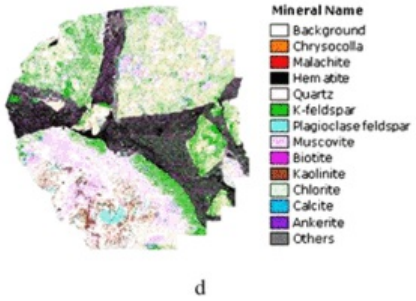

d

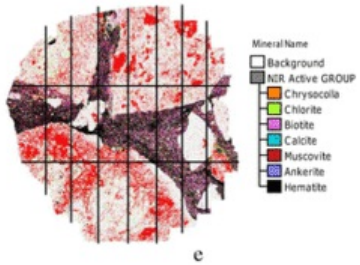

e

Fig. 9 (a–c) NIR spectra of sample no. 21. (d and e) The QEMSCAN® field scan image of sample no. 21 at 10 μm X-ray resolution, (d) all minerals present in the sample, (e) NIR active minerals shown only, vertical lines indicate pixel position while horizontal lines indicate spectral sectors on particles as scanned.

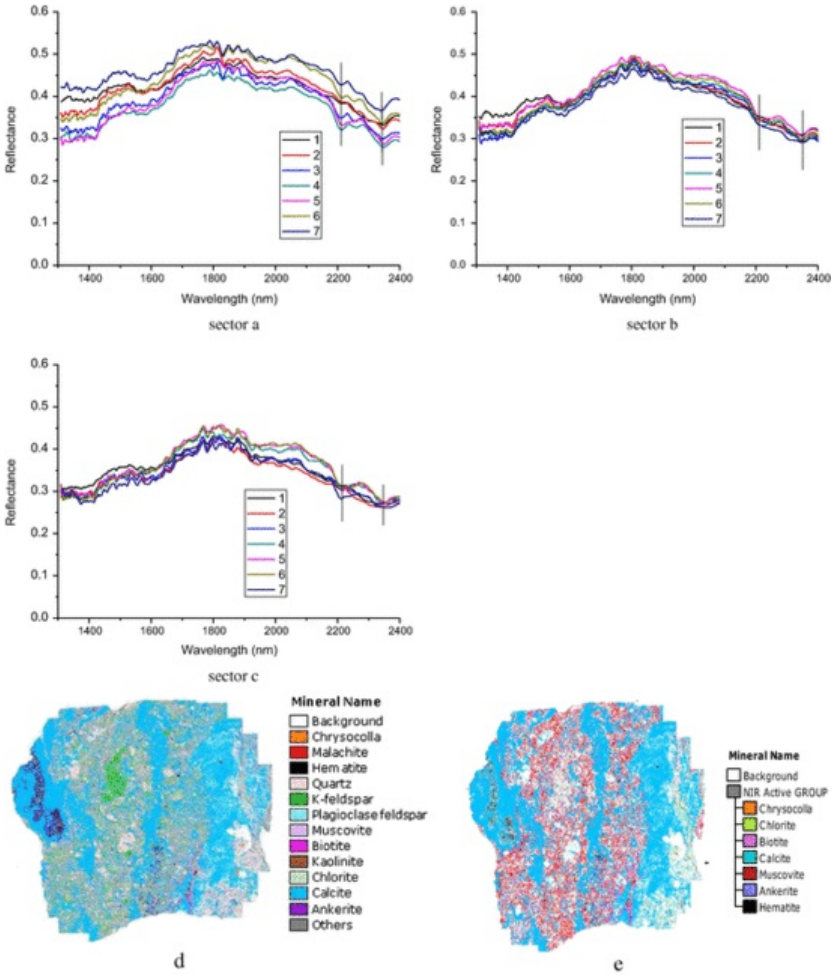

Fig. 10 (a–c) NIR spectra of sample no. 49. (d and e) QEMSCAN® field scan image of sample no. 49 at 10 µm X-ray resolution, (d) all minerals present in the sample, (e) NIR active minerals shown only, vertical lines indicate pixel position while horizontal lines indicate spectral sectors on particles as scanned.

Table 4 Classifications of split B1 samples, where P, M and W indicate product, middling and waste, respectively, M* and M-indicates middling with more product or waste pixels respectively.

Sample ID	Cu Content (Qem)%	Cu Content (PXRF)%	Classification					
			NIR(1)	NIR(2)	QEMSCAN	PXRF	Func(1)	Func(2)
			P	P	P	P	W	P
			P	P	P	P	W	P
2	6.46	2.59	P	P	P	P	W	P
3	7.33	7.74	P	P	P	P	W	P
4	1.75	1.37	P	P	P	P	P	P
5	1.70	1.77	P	P	P	P	W	P

6	0.41	0.58	P	P	W	P	W	W
7	0.05	0.12	P	P	W	W	W	P
8	1.90	0.61	P	P	P	P	P	P
9	2.28	1.89	P	P	P	P	W	W
10	3.55	1.05	M*(P)	P	P	P	P	P
11	3.15	3.93	M*(P)	P	P	P	P	P
12	2.34	1.98	P	P	P	P	P	P
13	0.00	0.03	M*(P)	P	W	W	W	W
14	0.40	0.97	M-(W)	P	W	P	W	P
15	0.00	0.03	M-(W)	P	W	W	W	W
16	0.14	0.12	M-(W)	M-(W)	W	W	W	P
17	1.41	0.72	P	P	P	P	W	P
18	0.09	0.04	W	P	W	W	W	P
19	0.15	0.32	P	P	W	W	W	W
20	0.36	0.12	P	P	W	W	W	P
21	0.02	0.10	M-(W)	P	W	W	W	P
22	0.03	0.03	P	P	W	W	W	P
23	0.02	0.04	P	P	W	W	W	P
24	0.80	0.15	W	P	P	W	P	P
25	0.12	0.13	P	P	W	W	W	W
26	1.81	2.02	P	P	P	P	W	P
27	0.00	0.02	W	P	W	W	W	W
28	0.92	0.75	P	P	P	P	W	P
29	0.07	0.06	W	P	W	W	W	W
30	0.03	0.07	P	P	W	W	W	P
31	0.09	0.09	P	P	W	W	W	P
32	1.23	0.34	P	P	P	W	W	P
33	0.00	0.02	M-(W)	P	W	W	W	W
34	0.07	0.05	P	P	W	W	W	P
35	1.71	2.16	M-(W)	M-(W)	P	P	W	W
36	0.01	0.03	M-(W)	P	W	W	W	W
37	0.28	0.17	P	P	W	W	W	P

38	0.06	0.22	P	P	W	W	W	P
39	0.33	0.16	P	P	W	W	W	P
40	0.30	0.15	P	P	W	W	W	P
41	0.00	0.04	P	P	W	W	W	W
42	0.09	0.11	M-(W)	P	W	W	W	W
43	0.01	0.08	W	M-(W)	W	W	W	W
44	0.05	0.08	P	P	W	W	W	W
45	0.18	0.11	P	P	W	W	W	W
46	0.04	0.08	M-(W)	M-(W)	W	W	W	W
47	0.54	0.27	M-(W)	M-(W)	P	W	W	W
48	1.40	1.44	P	P	P	P	P	P
49	0.14	0.09	W	W	W	W	W	W
50	11.54	4.08	P	P	P	P	W	P
51	1.00	1.49	P	P	P	P	W	W
52	0.01	0.14	M*(P)	P	W	W	W	W
53	0.01	0.05	W	P	W	W	W	W
54	0.06	0.35	M-(W)	P	W	W	W	W
55	3.28	7.64	W	P	P	P	W	W
56	0.05	0.05	W	W	W	W	W	W
57	2.77	4.87	W	P	P	P	W	W
58	0.00	0.05	P	P	W	W	W	P
59	0.03	0.20	P	P	W	W	W	P
60	1.98	1.96	P	P	P	P	P	P

A total of 23 NIR spectra were obtained from scans of sample no. 6 (Fig. 6a–c), the numbered horizontal and vertical line in Fig. 6e shows sectors and pixels positions on the sample as scanned by the NIR line scanner. The spectra of sample no. 6 show no absorption feature(s). Given the mineralogical composition of the sample, the lack of features is characteristic of hematite-dominated spectra (Iyakwari and Glass, 2015). Sample minerals data indicate calcite (17 wt%), and biotite (15 wt%) as the concentration dominant NIR-active minerals in sample no. 6 (Table 1). Despite their dominant concentration, their absorption features were dominated by hematite (10 wt%) which is seen as patches of dark minerals on the NIR-active minerals field scan image (Fig. 6e). The disseminated occurrence of hematite on the sample surface in addition to the fine grained nature of the sample makes other NIR-active minerals completely unable to display their own absorption features. This confirms findings reported by Iyakwari and Glass (2015). No mineral absorption features were visible in NIR spectra of intimate mixtures of minerals, even at calcite (or biotite) to hematite ratios of 9:1. Chlorite (7 wt%), is the other NIR-active mineral present in appreciable concentration. The chrysocolla concentration is small at 1 wt%.

Across all sectors, the spectra of sample no. 7 compare closely with the NIR spectra of the hematite dominated particle (Fig. 7a–c). A total of 23 NIR spectra were generated corresponding to 7, 8, and 8 per sector. The dominance of hematite on spectra is confirmed by sample mineral data (Table 1), which shows hematite (29 wt%) as the dominant mineral in the sample. Also, NIR-active minerals field scan image of the sample reveals patchy highly disseminated hematite across the sample face (Fig. 7e): this is responsible for the lack of features in the spectra of other NIR-active minerals in the sample. Hence, given the concentration and the spatially disseminated occurrence of hematite, biotite (13 wt%) and chlorite (9 wt%) cannot display their feature in the spectra.

A total of 24 spectra were generated from sample no. 9 (Fig. 8a–c). Though the sample mineral data (Table 1), show calcite having a concentration of 32 wt%, the NIR spectra appear to show no feature indicative of the presence of calcite in the sample.

Hematite is present in sample no. 9 with a concentration of 12 wt%. Thus both minerals (calcite and hematite) are at a ratio of 7:3. Hematite can also be seen on the sample's NIR-active minerals field scan image (Fig. 8e) occurring as disseminated patches highly mixed with calcite. Hence, given the ratio of both minerals and the disseminated occurrence of hematite over calcite, hematite is responsible for the absence/masking of calcite features in the spectra. The other NIR-active minerals in sample no. 9 with appreciable concentration and also unable to display features as a result of being masked by hematite (Iyakwari and Glass, 2015), are chlorite (14 wt%) and chrysocolla (4 wt%).

Sample no. 21 produced 24 NIR spectra (Fig. 9a–c). Of the 24 spectra, only 18 spectra display features near 1420 and 2210 nm, indicative of muscovite (Clark et al., 2007). The remaining six spectra, all in sector B, are featureless (Fig. 9b). Hence, the spectra reveal variation in the NIR-active mineralogical composition of the sample. Analysis of NIR-active minerals field scan images (Fig. 9e) show two distinct mineralogical compositions (muscovite and hematite) as displayed by the sample. Muscovite features can be observed in the spectra and showed strong occurrence in sectors A and C (Fig. 9a and c), while hematite is concentrated around the middle region sector B (Fig. 9b). The sample also reveals spatial association between hematite, biotite and chlorite, with patches of both minerals (biotite and chlorite) observed on hematite. With hematite, both minerals cannot display their absorption features within the NIR (Iyakwari and Glass, 2015). Though kaolinite occurs in sample no. 21 (~3 wt%), the spectra does not display absorption features diagnostic of kaolinite. Hence, kaolinite features are either masked by hematite or captured by muscovite. Mineralogical data show muscovite (19 wt%), hematite (19 wt%), biotite (5 wt%), chlorite (4 wt%), and kaolinite (3 wt%) as the NIR-active minerals in the sample.

The spectra of sample no. 49 across all sectors scanned show features near 2210 and 2345 nm (Fig. 10a–c). The 2210 nm feature belongs to muscovite while the 2345 nm feature are of calcite (Iyakwari and Glass, 2014). Mineralogical data and NIR-active mineral images (Table 1 and Fig. 10e) show calcite (42 wt%), muscovite (13 wt%) as the dominant NIR-active minerals in the sample. Biotite (3 wt%), chlorite (2 wt%), and hematite (2 wt%) are the other NIR-active minerals in the sample. The NIR spectra of sample no. 49 confirm the findings reported by Iyakwari and Glass (2015) where both minerals (muscovite and calcite) show features side-by-side even at lower muscovite concentration along all spectra.

4 Individual sample classification

The classification of individual splits B1 samples based on NIR (NIR (1) and (2)), PXRF and QEMSCAN® (Functional groups (Func. (1) and (2)) and Cu values (Qem)) data is presented in Table 4. Both elemental classifications (QEMSCAN® and PXRF) are based on a copper value of 0.5% and above as product.

5 Analysis of classification strategies

Table 4 shows that, based on QEMSCAN®-calculated Cu values (Qem), 23 samples (38% of total) were classified as product. The PXRF classified 22 samples (37% of total) as product. Based on the functional groups, Func. (1) considered 8 samples (13% of total) as product, while Func. (2), classified 17 samples as product (28% of total). Only 7 samples were classified by the NIR (2) as waste against 21samples classified as waste by NIR (1).

A comparison of NIR (1) and Qem classifications shows that only 5 samples (no. 24, 35, 47, 55 and 57) classified as waste by NIR (1) and product by Qem have a copper concentration above 0.5%. Also, 19 samples classified as product by the NIR (1) but wastes by Qem have copper concentration below 0.5%. Sample no. 6, 7, 13, 52, 58 and 59 were classified products by NIR (1) because of their high hematite content resulting to their featureless spectra. Sample no. 22, 30, 34, 37, 38, 39, 40, 44 and 45 were classified products because their spectra showed features corresponding to either chlorite/chrysocolla or biotite. The spectra of sample no. 23, 25, 31, and 41, appeared featureless across wavelength with a broad depression at longer wavelength lacking absorption centres. This is due to their complex spatial mineral associations: biotite–chlorite (sample no. 23), biotite–chlorite–calcite (sample no. 25 and 41) and biotite–chlorite–hematite (sample no. 31). Given their lack of any absorption feature(s) indicative of any mineral(s), the samples were classified as product.

The five samples classified as waste by NIR (1) but products by Qem strategy show absorption features diagnostic of either or both calcite and muscovite. Sample no. 24, 55 and 57 showed muscovite features near 2210 nm while sample no. 35 and 47 showed calcite features near 2340 nm. Mineralogically sample no. 24, 55 and 57 have muscovite concentration at 21.55 wt%, 18.87 wt% and 9.90 wt% respectively, with sample no. 55 and 57 also containing in addition to muscovite, calcite at 12.98 wt% and 17.08 wt%. Sample no. 35 and 47 have calcite concentration at 27.02 wt% and 22.64 wt% respectively (Table 1). Since their waste mineral content showed stronger absorption features than their product minerals concentration, they were classified as waste by NIR (1).

The matching of NIR (1) and PXRF classifications indicates that 18 out of 22 samples classified as product by PXRF were also classified as product by NIR, (i.e. 82% of total PXRF products samples). Hence, only four samples (no. 14, 35, 55, and 57) classified as product by PXRF were classified as waste by NIR (1). Three of the four NIR (1) waste samples (no. 35, 55 and 57) were classified by both PXRF and Qem as product because they were calibrated to classify sample based on their copper content. The Qem is not in agreement with the PXRF on sample no. 14, because both techniques differ on the sample's copper content, with the PXRF overestimating the Cu content in the particle (Table 4). NIR (1) classified sample no. 14 as waste because it showed muscovite features.

A comparison of NIR (1) and functional group classification (Func. 2) indicates that of the 17 samples classified as product by Func. 2, only one sample (sample no. 24) was classified as waste by NIR (1). Hence, except for sample no. 24, this classification indicates almost a 1:1 correlation for both techniques. This is true since both strategies are based on sample NIR-active minerals functional group(s) content. The NIR considered individual spectrum on the basis of the mineral(s) responsible for the absorption feature(s), while the Func. (2) strategy considered bulk functional group(s) per sample, ignoring the individual minerals responsible. Hence, sample no. 24 was classified as waste by NIR (1) because its spectra showed

muscovite features. NIR(1) classified 23 extra samples as products either due to their individual features indicating chlorite/chrysocolla or biotite, which are all –OH bearing or spectra appeared featureless. Only eight samples classified as product by Func. (1), out of which only sample no. 24 was classified waste by NIR (1).

Of all the NIR-active –OH bearing minerals in the copper ore samples, biotite contained the least –OH content of 7.54% closely followed by muscovite at 8.53% (Table 3). Muscovite displays strong absorption features in comparison to minerals like chrysocolla and chlorite that contain 20.71% and 22.85% –OH respectively (Iyakwari and Glass, 2015). Therefore, while sample no. 24 only contains a total of 2.77% of –OH as cumulative, which is below the –OH cut-off grade (5%) used in developing functional group strategy, the bulk of –OH was contributed by muscovite which has a concentration of 21.55 wt% (contributing approximately 1.8% –OH) occurring as the dominant NIR-active mineral in the particle. Also from NIR classification, all samples with hematite concentration (⩾10 wt%) classified either as product or as middlings. With exception of sample no. 14 and 21, which are further classified as waste due to their dominant waste spectra, all hematite-rich middling were classified as product.

Comparison of Func. (2) strategy and Qem data shows all 17 samples classified as product by Func. (2) are also classified by Qem as products. Hence, of the 23 samples having copper above 0.5%, only 6 samples (no. 9, 35, 47, 51, 55, and 57) were classified as waste by Func. (2). The basis of their classification as waste was due to their high CO_3^{2-} (sample no. 9 and 51) and/or CO_3^{2-} and –OH (sample no. 35, 47, 53 and 57) content. The same is true for Func. (1), except that 15 of the 23 Qem products were classified as waste by Func. (1).

5.1 Validation of NIR strategies

5.1.1 Splits B2

To calibrate and evaluate the applicability of classification strategies, samples of splits B2 (Fig. 1) were scanned and classified using the NIR strategies shown in Figs. 4 and 5. Elemental data obtained from powdered samples splits A1 (BPXRF), as well as data obtained from scanning splits B2 samples (PXRF) (Fig. 1) were used to compare the classifications (Table 5). Using strategy NIR (1), 41 samples were classified by NIR as product, while PXRF identified 35 samples as products using a copper cut-off grade of 0.5%. 29 of the 35 PXRF product samples were also classified as product by NIR (1) (i.e. 83% of total PXRF product samples). Therefore, only 6 samples classified as product by PXRF were classified as waste by NIR (1). The NIR spectra of sample no. 18, 54 and 55 shows only muscovite features, sample no. 35 shows only calcite features while sample no. 9, and 57 showed both muscovite and calcite features.

Table 5 Classifications of split B2 samples, where P, M and W indicate product, middling and waste, respectively. M* and M-indicates middling with more product or waste pixels respectively.

Sample ID	Cu content (BPXRF)%	Cu content (PXRF)%	Classification			
			BPXRF	PXRF	NIR(1)	NIR(2)
1	1.30	4.40	P	P	P	P
2	2.31	4.06	P	P	P	P
3	3.20	5.78	P	P	P	P
4	1.40	1.87	P	P	M*(P)	P
5	0.77	1.77	P	P	P	P
6	1.33	0.71	P	P	P	P
7	0.14	2.93	W	P	P	P
8	1.51	1.13	P	P	P	P
9	2.82	2.71	P	P	W	W
10	8.66	10.95	P	P	P	P
11	8.91	8.91	P	P	P	P
12	1.85	0.85	P	P	P	P
13	0.18	0.03	W	W	M-(W)	M-(W)

14	0.49	1.52	W	P	M*(P)	P
15	0.03	0.03	W	W	M-(W)	P
16	0.35	1.31	W	P	P	P
17	0.34	2.04	W	P	P	P
18	0.13	4.39	W	P	M-(W)	P
19	0.25	0.61	W	P	P	P
20	0.18	0.65	W	P	P	P
21	0.09	0.17	W	W	M*(P)	P
22	0.08	0.62	W	P	P	P
23	0.09	2.58	W	P	P	P
24	3.30	0.14	P	W	M-(W)	P
25	0.74	0.33	P	W	M-(W)	M-(W)
26	0.45	0.88	W	P	P	P
27	0.02	0.05	W	W	W	W
28	0.73	0.30	P	W	P	P
29	0.10	0.09	W	W	W	P
30	0.24	0.15	W	W	P	P
31	0.22	0.46	W	W	P	P
32	0.89	0.88	P	P	P	P
33	0.03	0.07	W	W	P	P
34	0.21	0.21	W	W	P	P
35	0.89	2.13	P	P	W	W
36	0.06	0.14	W	W	P	P
37	0.12	1.42	W	P	P	P
38	0.22	0.69	W	P	P	P
39	0.14	0.16	W	W	M*(P)	M*(P)
40	0.44	1.78	W	P	P	P
41	0.05	0.03	W	W	P	P
42	0.11	0.25	W	W	W	W
43	0.13	1.31	W	P	M*(P)	M*(P)
44	0.21	5.88	W	P	P	P
45	0.11	2.01	W	P	P	P

46	0.16	0.11	W	W	W	W
47	0.46	0.17	W	W	W	W
48	0.36	0.43	W	W	M*(P)	M*(P)
49	0.13	0.31	W	W	M-(W)	P
50	2.08	3.87	P	P	P	P
51	1.39	0.67	P	P	P	P
52	0.14	0.11	W	W	W	W
53	0.09	0.09	W	W	W	W
54	0.23	0.65	W	P	W	P
55	3.03	3.93	P	P	W	P
56	0.33	0.17	W	W	W	W
57	2.28	1.02	P	P	W	W
58	0.07	0.09	W	W	P	P
59	0.19	0.18	W	W	P	P
60	4.44	1.97	P	P	P	P

The second strategy, NIR (2), classified only 12 samples as waste, compared to the 19 samples classified as waste by the NIR (1). Hence, product concentrate by NIR (2) consist of 48 samples.

6 Evaluation of results

Ore parameters for each split were calculated based on the assumption that the mass of each sample were the same.

6.1 Splits B1

Classification of 60 samples is presented in Table 4. Tables 6a and 6b present calculated parameters of splits B1.

Table 6a Comparison of discrimination results of splits B1, using copper content calculated from copper-bearing minerals Qem.

	NIR (1)	NIR (2)	Qem	Func. (1)	Func. (2)
Content of copper in feed, %	1.12	1.12	1.12	1.12	1.12
Content of copper in product, %	1.47	1.22	2.77	2.11	3.06
Content of copper in waste, %	0.49	0.38	0.10	0.97	0.36
Recovery of Cu in product, %	85	96	94	25	77
Yield of product, %	65	88	38	13	28

Table 6b Comparison of discrimination results of splits B1, using copper content measured by PXRF.

	NIR (1)	NIR (2)	PXRF	Func. (1)	Func. (2)
Content of copper in feed, %	0.96	0.96	0.96	0.96	0.96

Content of copper in product, %	1.03	1.03	2.42	1.56	2.00
Content of copper in waste, %	0.82	0.41	0.11	0.87	0.54
Recovery of Cu in product, %	70	95	93	21	59
Yield of product, %	65	88	37	13	28

Comparing *NIR (2)* and *Func. (2)*, where only calcite was targeted, showed an improvement in copper recovery and overall yield. An improvement of 11% and 23% was achieved using copper values from Qem, while 52% and 12% is achieved for *Func 2* (Table 6a). Also achieved was a reduction in copper content reporting to waste from 0.49% for *NIR (1)* to 0.38% for *NIR (2)* and from 0.97% for *Func. (1)* to 0.36% for *Func. (2)*. The same was true for values calculated by PXRF. The PXRF showed reduction of 50% of the total copper reporting to waste for *NIR (1)*, with improvement in copper recovery of 25% (Table 6b). Similar improvement was achieved for *Func. (2)* against *Func. (1)*.

6.2 Splits B2

Classification of splits B2 samples is presented in Table 5.The calculated parameters are presented in Tables 7a and 7b using data from PXRF and BPXRF respectively.

Table 7a Comparison of discrimination results of splits B2, using copper content measured by PXRF.

	NIR (1)	NIR (2)	PXRF
Content of copper in feed, %	1.55	1.55	1.55
Content of copper in product, %	1.87	1.79	2.54
Content of copper in waste, %	0.88	0.60	0.17
Recovery of Cu in product, %	82	92	95
Yield of product, %	68	80	58

Table 7b Comparison of discrimination results of splits B2, using copper content measured on powdered samples by PXRF.

	NIR (1)	NIR (2)	BPXRF
Content of copper in feed, %	1.02	1.02	1.02
Content of copper in product, %	1.12	1.10	2.56
Content of copper in waste, %	0.80	0.68	0.19
Recovery of Cu in product, %	80	87	88
Yield of product, %	68	80	35

Comparison of calculated parameters indicates improvement in both yield and recovery by 12% and 10% respectively for *NIR (2)* as when using PXRF values with a reduction of 0.28% of copper reporting to waste from 0.88% to 0.60% (Table 7a). The same was true using values from BPXRF (Table 7b), showing an improvement of 7% in recovery and 12% in yield.

7 Implication of NIR sorting

Since the purpose of mineral processing is to increase the economic value of an ore, the economics of any processing method or strategy must be considered prior to its application (Wills and Napier-Munn, 2006). Improving the economic value or upgrading an ore is assumed to be economical when it is achieved using the cheapest and most efficient available method and or strategy. While minimizing the amount of ore mineral that reports to gangue is a major consideration, the recovery is critical.

The aim of using NIR as a preconcentration method is to upgrade the ore by reducing the quantity of overall waste material reporting to the next processing stage. This is achieved by eliminating/reducing the waste fraction, in this ore the calcite and or clay (muscovite/kaolinite) rich particles. These are the only groups of waste minerals that can be targeted by NIR since other non-copper-bearing minerals like chlorite, biotite and hematite cannot be effectively discriminated from

chrysocolla (Iyakwari and Glass, 2015). Since the NIR range used (1300 to 2400 nm) does not sense copper signature (Iyakwari et al., 2013), the NIR classification was correlated with data from portable XRF and Cu values calculated from Cu-bearing minerals (chrysocolla, malachite and cuprite) as analysed by QEMSCAN®. The elemental/mineralogical data was then used to determine the economic/metallurgical implication of NIR application and the individual sample classifications based on NIR, functional groups content as well as copper content are compared.

Based on potential for NIR discrimination, two strategies were employed. The first strategy, NIR(1), considered the elimination of both calcite and muscovite as wastes, while the second strategy, NIR (2), was aimed at eliminating only calcite as waste. With the first strategy, the calculated data of product fractions for split B1 (Tables 6a and 6b), and split B2 (Table 7a and 7b) indicated that the calculated recovery of copper was higher in PXRF and Qem than NIR and Func. This is because the copper content was considered with no consideration for their carbonate and hydroxyl content. Therefore, while the NIR and Func classified sample material on the ore quality only, PXRF and Qem classification was based on the quantity of copper in a sample. Also observed from NIR (1) and Func. (1) was the high percentage of copper lost to waste, in most cases with values higher than the assumed cut-off grade (0.5%).

Copper recoveries from NIR (2) and Func. (2) revealed a marked improvement from those obtained from NIR (1) and Func. (1). The second strategies also achieved higher copper recovery when compared to Qem and PXRF strategies. Results of the second strategy revealed that copper in form of chrysocolla are locked in muscovite-dominated spectra or spectrum using NIR (1). Hence, eliminating both calcite and muscovite will amount to loss of valuable as waste. Therefore, in terms of economic of copper recovery, the second strategies provided better options for consideration and application in preconcentrating the copper ore, as samples reporting to waste are only samples with known calcite concentration containing little or no chrysocolla. Therefore, although the first strategy provides fairly pure concentrate, the second strategy minimizes the loss of valuable as waste.

Though both NIR and Func classified samples based on functional groups, the higher recovery achieved by NIR over Func in both strategies revealed that NIR holds a good potential in its ability to classify even lower grade samples as products provided those samples show no calcite and or clay minerals absorption features.

Reduction of the total amount of dominantly waste bearing material through NIR preconcentration using either strategies (NIR (1) or NIR (2)) decreases the amount of money spent on acid and comminution (especially grinding). While this could constitute up to 50% of the total energy cost used in mineral processing operation (Wills and Napier-Munn, 2006), the total volume of the waste rejection leads to a proportional reduction in the total energy cost.

8 Conclusions

A NIR sensor, which does not measure elemental concentrations, was used in this research as a method of qualitative analysis for preconcentrating complex ores. NIR techniques or strategies enabled particles with variation in mineralogy to be classified as middling and recommended for further liberation where applicable before re-scanning. The NIR sensor strategies allow the discrimination of a significant amount of material at a copper grade that is less than half the assumed economic cut-off-grade of 0.5%. This indicates that there is potential that the NIR sensor based sorting can provide economic benefits for processing ore.

QEMSCAN® field scan images showed how individual mineral crystals or grains appear in a particle and are sensed by NIR. The comparison was possible because both the NIR and the QEMSCAN® have nearly similar depth of particle penetration. The difference between these methods is that, while the NIR sees only NIR-active minerals, QEMSCAN® identifies all minerals present in a sample, with an elemental detection limit of about 3% per analysis point. The advantage NIR has over QEMSCAN® is its ability to detect NIR-active functional groups in minerals (H_2O, –OH and CO_3^{2-}) quickly without rigorous sample preparation.

Comparison of XRD and NIR revealed that the NIR spectra of some samples showed features of minerals not detected by XRD. Thus, implying that the NIR has a better detection limit compared to XRD and as such NIR detects minerals structure at a smaller scale than XRD, making measurement of low-crystallinity minerals possible. Another advantage of NIR over XRD is its ability to detect amorphous minerals presence in a sample provided they are NIR-active.

Based on combined use of NIR, QEMSCAN® (mineralogy/functional groups and calculated Cu values), PXRF and XRD, a system of calibration was developed which allows upgrading of the ore through gangue removal. The information provided here could be used for both mineralogical and metallurgical purposes aimed towards improving copper recovery, reducing acid consumption, and reducing operational cost in terms of energy consumption through less ore needing to be processed.

9 Uncited references

Andresen et al. (2009), Clark et al. (1990), Clark (1999), Halbich (1934).

Acknowledgments

We wish to thank Anglo American for providing the samples. The Nigerian Government, through the academic staff support scheme of the Tertiary Education Trust Fund of Nigeria (TETFON), and the Management of Nasarawa State University, Keffi, are acknowledged for providing financial support for this research.

References

ELSEVIER_MINE_4780

Anderson K.F., Wall F., Rollinson G.K. and Moon C.J., Quantitative mineralogical and chemical assessment of the Nkout iron ore deposit, Southern Cameroon, *Ore Geol. Rev.* **62**, 2014, 25–39Bishop, J. L., Dummel, A., 1996. The influence of fine-grained hematite powder on the spectral properties of Mars soil analogs; VIS-NIR bi-directional reflectance spectroscopy of mixtures. *Lunar and Planetary Institute Science Conference Abstracts*, Vol. 27Bokobza L., Near infrared spectroscopy, J. Near Infrared Spectrosc., 6, 1998, 3-7..

Andresen J.C.O., Rollinson G.K., Snook B., Herrington R. and Fairhurst J.R., Use of QEMSCAN® for the characterization of Ni-rich and Ni-poor goethite in laterite ores, *Miner. Eng.* **22**, 2009, 1119–1129.

Clark R.N., King T.V.V., Klejwa M., Swayze G.A. and Vergo N., High spectral resolution reflectance spectroscopy of minerals, *J. Geophys. Res.* **95**, 1990, 12653–12680 (Reference cited in the text).

Clark R.N., Reflectance spectra, In: Ahrens T.J., (Ed), *Rock Physics and Phase: A Handbook of Physical Constants,* 1995, American Geophysical Union; Washington, 178–188Clark, R.N., Swayze, G.A., Wise, V., Livo, K.E., Hoefen, T.M., Kokaly, R.F., Sutley, S.J., 2007. USGS digital spectral library splib06a: U.S. Geological Survey, Data Series 231..

Clark R.N., Spectroscopy of rocks and minerals, and principles of spectroscopy, In: Rencz N., (Ed), *Remote Sensing for the Earth Sciences: Manual of Remote Sensing* **vol. 3**, 1999, John Wiley & Sons; New York, 3–52.

Coates J., Interpretation of infrared spectra, a practical approach, In: Meyers R.A., (Ed), *Encyclopaedia of Analytical Chemistry,* 2000, Wiley & Sons Ltd.; Chichester, 10815–10837.

Curtis B., Developing automated copper ore processing using NIR analysis and XRD, *Adv. Mater. Processes* **170** (2), 2012, 24–26.

Dalm M., Buxton M.W., van Ruitenbeek F.J. and Voncken J.H., Application of near-infrared spectroscopy to sensor based sorting of a porphyry copper ore, *Miner. Eng.* **58**, 2014, 7–16.

Gaydon, J.W., 2011. The Application of a Near-Infrared Sensor to Sorting of Minerals. (Ph.D. thesis). Camborne School of Mines, University of Exeter, Penryn Campus, United Kingdom.Gaydon J.W., Glass H.J. and Pascoe R.D., Method for near infrared sensor-based sorting of a copper ore, *J. Near Infrared Spectrosc.* **17**, 2009, 177–194.

Gottlieb P., Wilkie G., Sutherland D., Ho-Tun E., Suthers S., Perera K., Jenkins B., Spencer S., Butcher A. and Rayner J., Using quantitative electron microscopy for process mineralogy applications, *JOM* **52** (4), 2000, 24–25.

Gupta K.C., Chemical Metallurgy: Principles and Practice, 2003, WILEY-VCH Verlag GmbH & Co; Weinheim. ISBN: 3-527-30376-6.

Habashi F., Handbook of extractive metallurgy. Vol. II: primary metals, secondary metals, *Light Metals* 1997, WILEY-VCH; Weinheim, ISBN: 3-527-28792-2.

Halbich W., Über die AnwendungsmöglichkeiteneinigerNetzmittel in der Flotation, 1934, KondradTriltsch; Würzburg.

Hunt G.R., Spectral signatures of particulate minerals in the visible and near-infrared, *Geophysics* **42** (3), 1977, 501–513.

Iyakwari S., Glass H.J. and Kowalczuk P.B., Potential for near infrared sensor-based sorting of hydrothermally-formed minerals, *J. Near Infrared Spectrosc.* **21** (3), 2013, 223–229.

Iyakwari S. and Glass H.J., Influence of mineral particle size and choice of suitable parameters for ore sorting using near infrared sensors, *Miner. Eng.* **69**, 2014, 102–106.

Iyakwari S. and Glass H.J., Mineral preconcentration using near infrared sensor-based sorting, *Physicochem. Probl. Miner. Process.* **51** (2), 2015, 661–674.

Li L., Wu Q., Li S. and Wu O., Study of the infrared spectral features of an epoxy curing mechanism, *Appl. Spectrosc.* **62** (10), 2008, 1129–1136.

Pasquini C., Near infrared spectroscopy: fundamentals, practical aspects and analytical applications, *J. Braz. Chem. Soc.* **14** (2), 2003, 198–219.

Pirrie D. and Rollinson G.K., Unlocking the applications of automated mineral analysis, *Geol. Today* **27** (6), 2011, 235–244.

Povarennykh A.S., The use of infrared spectra for the determination of minerals, *Am. Mineral.* **63**, 1978, 956–959.

Reich G., Near-infrared spectroscopy and imaging: basic principles and pharmaceutical application, *Adv. Drug Deliv. Rev.* **57**, 2005, 1109–1143.

Robb L., 2005. Introduction to Ore-Forming Processes, Wiley-Blackwell. ISBN: 978-0-632-06378-9Van der Meer, F., Spectral reflectance of carbonate mineral mixtures and bidirectional reflectance theory: Quantitative analysis techniques for application in remote sensing, Rem. Sens. Rev. **13**, 1995, 67-94Wills B.A. and Napier-Munn T., Mineral processing technology, seventh ed., *An Introduction to the Practical; Aspects of ore Treatment and Mineral* 2006, Elsevier Sci. & Tech. Book, ISBN: 0750644508.

Graphical abstract

ELSEVIER_MINE_4780

Copper samples preconcentration strategy targeted at eliminating only calcite-bearing samples as waste.

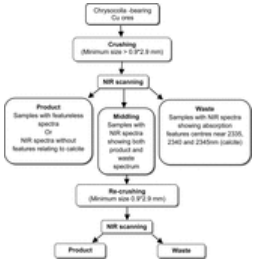

Highlights

- Combination of near infrared and QEMSCAN technologies to aid ore recovery.
- Near infrared discrimination correlates well with mineralogical and chemical classifications.
- Preconcentration of copper ore by near infrared sensor-based sorting is proposed.

Queries and Answers

Query: Your article is registered as a regular item and is being processed for inclusion in a regular issue of the journal. If this is NOT correct and your article belongs to a Special Issue/Collection please contact n.rajaj@elsevier.com immediately prior to returning your corrections.
Answer: yes it is a regular item

Query: Please confirm that given name(s) and surname(s) have been identified correctly.
Answer: they are all correct

Query: References ‘Robb (2005)’, ‘Gaydon (2011)’, ‘Bokobza (1998)’, ‘Clark et al. (2007)’, ‘Van Der Meer (1995)’, and ‘Bishop and Dummel (1996)’ are cited in the text but not provided in the reference list. Please provide them in the reference list or delete these citations from the text.
Answer: References inserted

Query: Please check the hierarchy of the section headings.
Answer: checked and are all correct

Query: This section comprises references that occur in the reference list but not in the body of the text. Please position each reference in the text or, alternatively, delete it. Any reference not dealt with will be retained in this section.
Answer: All deleted